

A new viable region of the inert doublet model

Laura Lopez Honorez*

Service de Physique Théorique, Université Libre de Bruxelles, 1050 Brussels, Belgium

Carlos E. Yaguna†

Departamento de Física Teórica C-XI and Instituto de Física Teórica UAM-CSIC,
Universidad Autónoma de Madrid, Cantoblanco, E-28049 Madrid, Spain

Abstract

The inert doublet model, a minimal extension of the Standard Model by a second Higgs doublet, is one of the simplest and most attractive scenarios that can explain the dark matter. In this paper, we demonstrate the existence of a new viable region of the inert doublet model featuring dark matter masses between M_W and about 160 GeV. Along this previously overlooked region of the parameter space, the correct relic density is obtained thanks to cancellations between different diagrams contributing to dark matter annihilation into gauge bosons (W^+W^- and Z^0Z^0). First, we explain how these cancellations come about and show several examples illustrating the effect of the parameters of the model on the cancellations themselves and on the predicted relic density. Then, we perform a full scan of the new viable region and analyze it in detail by projecting it onto several two-dimensional planes. Finally, the prospects for the direct and the indirect detection of inert Higgs dark matter within this new viable region are studied. We find that present direct detection bounds already rule out a fraction of the new parameter space and that future direct detection experiments, such as Xenon100, will easily probe the remaining part in its entirety.

1 Introduction

The identification of the dark matter particle is one of the most challenging problems in astroparticle physics today. We know that dark matter exists, for the evidence in its favor is varied and overwhelming. It comes, among others, from rotation curves in galaxies, gravitational lensing effects in clusters of galaxies, the large scale structure of the Universe, and the Cosmic Microwave Background (CMB). The anisotropies in the CMB, in fact, indicate that while dark matter accounts for about 23% of the energy density of the Universe, baryonic matter reaches only around 4% [1]. Most of the matter in the Universe, therefore, is in the form of dark matter. And yet we still ignore what dark matter consists of.

Currently there is a huge experimental effort aimed at detecting the dark matter particle and determining its main properties. Dark matter particles can be detected, for example, via nuclear recoil as they scatter off nuclei in *direct* detection experiments. In recent years, direct detection

*llopezho@ulb.ac.be

†carlos.yaguna@uam.es

experiments such as CDMS [2] or Xenon [3] have been continuously improving the constraints on the spin-independent dark matter-nucleon cross section, and they have started to probe interesting regions of the parameter space of common dark matter models. The *indirect* detection of dark matter, which relies on the annihilation of dark matter particles rather than on their scatterings, is another promising avenue toward the identification of the dark matter. Dark matter annihilations may produce photons, antimatter (positrons and antiprotons mainly) and neutrinos that can be detected as exotic components in cosmic rays. At present, several experiments including FERMI (photons) [4], PAMELA (antimatter) [5] and ICECUBE (neutrinos) [6] are already taking data and setting some constraints on the dark matter properties. Finally, dark matter particles or other particles associated with it may also be produced and detected in colliders such as the LHC. It may be that the LHC soon finds evidence of physics beyond the Standard Model that sheds some light on the dark matter puzzle.

In parallel with this experimental effort, there has been a lot of interest in the theoretical aspects of dark matter. Even though extremely successful in describing collider experiments, the Standard Model of particle physics does not include any viable dark matter candidate. Dark matter, therefore, provides compelling evidence for the existence of new physics, of physics beyond the Standard Model. Over the years, many dark matter candidates have been proposed in different scenarios for physics beyond the Standard Model. They include the neutralino [7] and the gravitino [8] in supersymmetric models, the lightest Kaluza-Klein particle in Universal Extra Dimensional models [9], as well as the singlet scalar [10] or the inert Higgs [11–18] that appear in minimal extensions of the Standard Model. Thanks to the simplicity of the underlying model and to the rich phenomenology associated with it, the inert Higgs –the lightest odd particle of the inert doublet model– has earned a special place among them as one of the most attractive dark matter candidates considered in the recent literature.

In the inert doublet model, a Higgs doublet H_2 , odd under a new Z_2 symmetry, is added to the Standard Model particle content. The lightest inert (odd) particle, H^0 , turns out to be stable and hence a suitable dark matter candidate. After being introduced in [11], this model has been extensively studied in a number of recent works [12–18]. In [12], it was extended with odd right-handed neutrinos so as to explain neutrino masses. Then, in [13], it was proposed as a possible way to increase the Higgs mass without contradicting electroweak precision data. Regarding dark matter, the main features of the model were systematically analyzed in [14]. Later on, in [15], it was shown that the annihilation of inert Higgs dark matter can give rise to significant gamma ray lines. Recently, it was demonstrated that, for masses between 60 GeV and M_W , dark matter annihilations are usually dominated by three-body final states consisting of a real and a virtual W [19, 20], rather than by the two-body final states considered in previous works. A result that has important implications for the determination of the viable parameter space of the model and for the detection prospects of inert Higgs dark matter.

These various studies have established that in the inert doublet model the dark matter constraint can only be satisfied within specific regions of the parameter space. Three viable regions have been identified: a low mass regime, with $M_{H^0} \lesssim 50$ GeV, where dark matter annihilates exclusively into fermion pairs; an intermediate mass regime, with $M_{H^0} \lesssim M_W$, where dark matter annihilations are dominated by the final states WW^* and $b\bar{b}$, and where coannihilations with A^0 may also play a role in the determination of the relic density; and a heavy mass regime, $M_{H^0} \gtrsim 500$ GeV, where the annihilation into gauge bosons is dominant and the mass splitting between the inert particles is small.

We demonstrate in this paper the existence of another viable region of the inert doublet model,

a region that had been overlooked in previous analysis. This region features dark matter masses between M_W and about 160 GeV and is compatible with the relic density constraint thanks to cancellations among the different diagrams that contribute to dark matter annihilation into gauge bosons. It is our goal to introduce this new viable region and to analyze its main properties. We determine its position in the multidimensional parameter space of the inert doublet model and study its implications for the direct and indirect detection of inert Higgs dark matter. Remarkably, we find that this new viable region will be entirely and easily probed by the next generation of direct dark matter detection experiments such as Xenon100.

In the next section, the inert doublet model is briefly reviewed, with particular emphasis on the different bounds that must be taken into account. Then, we describe in some detail the known viable regions of the model, those that are compatible with the observed dark matter abundance and with all other experimental and theoretical constraints. In section 4, we illustrate, analytically and numerically, the existence of cancellations in the annihilation of inert Higgs dark matter into W^+W^- and Z^0Z^0 that allow to satisfy the relic density constraint for dark matter masses above M_W . The effect of the different parameters of the model on these cancellations and on the predicted relic density are studied, and several examples of models within the new viable region are provided. In section 5, we use Markov Chain Monte Carlo techniques to scan the parameter space of the inert doublet model and obtain a large sample of models within the new viable region. We then determine the main features of this region by projecting this multidimensional cloud of viable models onto several two-dimensional planes. The issue of the fine-tuning required to obtain the correct relic density is also addressed, and it is found that these models are not particularly fine-tuned. Finally, we consider, in section 6, the detection prospects of inert Higgs dark matter in direct and indirect detection experiments.

2 The inert doublet model

The inert doublet model is a simple extension of the Standard Model with one additional Higgs doublet H_2 and an unbroken Z_2 symmetry under which H_2 is odd while all other fields are even. This discrete symmetry prevents the direct coupling of H_2 to fermions and, crucial for dark matter, guarantees the stability of the lightest inert particle. The scalar potential of this model is given by

$$V = \mu_1^2 |H_1|^2 + \mu_2^2 |H_2|^2 + \lambda_1 |H_1|^4 + \lambda_2 |H_2|^4 + \lambda_3 |H_1|^2 |H_2|^2 + \lambda_4 |H_1^\dagger H_2|^2 + \frac{\lambda_5}{2} \left[(H_1^\dagger H_2)^2 + \text{h.c.} \right], \quad (1)$$

where H_1 is the Standard Model Higgs doublet, and λ_i and μ_i^2 are real parameters. As in the Standard Model, λ_1 and μ_1^2 can be traded for the Higgs mass, M_h , and the vacuum expectation value of H_1 , $v = 246$ GeV¹. Four new physical states are obtained in this model: two charged states, H^\pm , and two neutral ones, H^0 and A^0 . Either of them could be dark matter. In the following we choose H^0 as the lightest inert particle, $M_{H^0}^2 < M_{A^0}^2, M_{H^\pm}^2$, and, consequently, as the dark matter candidate. After electroweak symmetry breaking, the inert scalar masses take

¹Notice that in [13] a different convention, $v = 174$ GeV, is used.

the following form

$$M_{H^\pm}^2 = \mu_2^2 + \frac{1}{2}\lambda_3 v^2, \quad (2)$$

$$M_{H^0}^2 = \mu_2^2 + \frac{1}{2}(\lambda_3 + \lambda_4 + \lambda_5)v^2, \quad (3)$$

$$M_{A^0}^2 = \mu_2^2 + \frac{1}{2}(\lambda_3 + \lambda_4 - \lambda_5)v^2. \quad (4)$$

Notice that λ_5 determines the mass splitting between M_{H^0} and M_{A^0} and is necessarily negative as $M_{A^0} > M_{H^0}$. The mass splitting between the charged and the neutral components, on the other hand, is due to both λ_4 and λ_5 . It is convenient to trade for μ_2^2 the parameter λ_L defined by

$$\lambda_L \equiv \frac{\lambda_3 + \lambda_4 + \lambda_5}{2} = \frac{M_{H^0}^2 - \mu_2^2}{v^2}. \quad (5)$$

As we will see, this parameter, which determines the interaction term between a pair of H^0 and the Higgs boson, will play a crucial role in the cancellations discussed in Section 4. The free parameters of the inert doublet model can then be taken to be the following:

$$M_{H^0}, M_{H^\pm}, M_{A^0}, M_h, \text{ and } \lambda_L. \quad (6)$$

From them the λ_i and μ_i^2 parameters appearing in the scalar potential, equation (1), can be reconstructed via equations (2-5).

These parameters are subject to a number of theoretical and experimental constraints –see [13] and [14]. To prevent the breakdown of perturbation theory, the λ_i parameters cannot be very large. We demand accordingly that

$$|\lambda_i| < 4\pi. \quad (7)$$

The requirement of vacuum stability, in addition, imposes the following conditions on the λ_i parameters:

$$\lambda_1, \lambda_2 > 0, \quad \lambda_3, \lambda_3 + \lambda_4 - |\lambda_5| > -2\sqrt{\lambda_1 \lambda_2}. \quad (8)$$

Since λ_2 only affects the quartic interaction term among the inert particles, the phenomenology of the model is rather insensitive to its precise value. For definiteness we set $\lambda_2 = 3.0$ throughout this work and use the above equation as a constraint on the remaining parameters of the model.

Accelerator bounds should also be taken into account. The mass of the charged scalar, M_{H^\pm} , is constrained to be larger than 70 – 90 GeV [21]; $M_{H^0} + M_{A^0}$ must exceed M_Z to be compatible with the Z^0 -width measurements; and some regions in the plane (M_{H^0}, M_{A^0}) are constrained by LEP II data [17]. Another important restriction on the parameter space of the inert doublet model comes from electroweak precision data. The inert doublet, H_2 , contributes to electroweak precision parameters such as S and T . It turns out that its contribution to S is always small [13], so it can be neglected. Its contribution to T , ΔT , was computed in [13] and is given by

$$\Delta T = \frac{1}{16\pi^2 \alpha v^2} [F(M_{H^\pm}, M_{A^0}) + F(M_{H^\pm}, M_{H^0}) - F(M_{A^0}, M_{H^0})] \quad (9)$$

where

$$F(m_1, m_2) = \frac{m_1^2 + m_2^2}{2} - \frac{m_1^2 m_2^2}{m_1^2 - m_2^2} \ln \frac{m_1^2}{m_2^2}. \quad (10)$$

This contribution originates in the $\lambda_{4,5}$ terms in the potential, for those are the terms breaking the custodial symmetry. The Higgs mass, M_h , also affects T via [22]

$$T_h \approx -\frac{3}{8\pi \cos^2 \theta_W} \ln \frac{M_h}{M_Z}. \quad (11)$$

For large M_h this contribution violates current experimental constraints. In fact, if no new physics affects the electroweak precision parameters, M_h should be smaller than 186 GeV at 95% C.L. In the inert doublet model, however, there is certainly physics beyond the Standard Model, so it is possible to have a heavier Higgs boson provided that the inert particles give rise to a positive compensating ΔT . In fact, the Higgs boson can be as heavy as 600 GeV in the inert doublet model [13].

It is useful to differentiate a light and a heavy Higgs regime in this model. In the heavy Higgs regime, $M_h > 200$ GeV, ΔT should be positive and equation (9) implies that $M_{H^\pm} > M_{A^0}$. In the light Higgs regime ($M_h < 200$ GeV), on the contrary, there is no correlation between M_{H^\pm} and M_{A^0} .

In our numerical analysis we implement the electroweak precision constraint by requiring that

$$-0.1 < \Delta T + T_h < 0.2, \quad (12)$$

in agreement with present bounds [23].

Finally, since dark matter is the most compelling motivation of the inert doublet model, we also constrain the relic density of inert Higgs dark matter to be compatible with the observed dark matter density. Explicitly we impose that

$$0.09 < \Omega h^2 < 0.13, \quad (13)$$

which is consistent with the WMAP measurement [1]. To ensure that the relic density of inert Higgs dark matter is accurately computed, we make use of the micrOMEGAs package [24] throughout this work.

As expected, all these constraints can be satisfied only within certain regions of the parameter space, the so-called *viable* regions. Before describing the new viable region of the inert doublet model –the main topic of this paper–, we will have a look in the next section to the previously known viable regions.

3 The known viable regions

In previous works [13, 14, 25, 26], it has been found that the dark matter constraint can only be satisfied for restricted values of M_{H^0} . Three viable regions can be distinguished: a small mass regime, with $M_{H^0} \lesssim 50$ GeV; a large mass regime, where $M_{H^0} > 500$ GeV; and an intermediate mass regime where $50 \text{ GeV} \lesssim M_{H^0} < M_W$.

In the small mass range, A^0 and H^\pm must be decoupled from H^0 in order to satisfy collider and precision test constraints. Thus, the inert doublet model becomes equivalent (for dark matter purposes) to the singlet scalar model of dark matter [10]. Dark matter annihilations proceed in this case through Higgs mediated diagrams into light fermions and are therefore dominated by the $b\bar{b}$ final state. Interesting phenomenological issues related to this mass range, including prospects for the direct and the indirect detection of dark matter, were studied in [26–30]. Recently, this

small mass regime of the inert doublet model, in particular the region $M_{H^0} \sim 8$ GeV, received some attention given the results of DAMA [31] and Cogent [32] experiments.

On the other edge of the mass range, the high mass regime, between 535 GeV and 50 TeV, is quite generic for scalar candidates of minimal dark matter models [25]. A detailed analysis of this mass range was given in [33]. They found that to satisfy the WMAP constraint, a small mass splittings between the components of the inert doublet is required, $\Delta M < 20$ GeV. In this case, dark matter annihilates mainly into W^+W^- , Z^0Z^0 and hh . Previous analysis, including prospects for dark matter detection, were presented in [14, 25, 28–30]. A more recent study showed that the high mass regime of the inert doublet could be responsible for the DAMA signal through inelastic scattering [29].

The intermediate mass regime, $M_{H^0} \lesssim M_W$, is a particular feature of the inert doublet model which can not be reproduced in any other of the $SU(2)_L$ minimal dark matter scalar models. For these masses, dark matter annihilations are dominated by $b\bar{b}$ and by the three-body final state WW^* , and the correct relic abundance can be obtained with or without coannihilations between H^0 and A^0 (collider constraints on new charged particles prevent coannihilations with H^\pm). Given the richness and the simplicity of the physics involved, various studies have been devoted to the inert doublet model in this precise mass range. The first analysis of this parameter space were carried out in [13, 14]. Further on, it was shown that the annihilation of inert Higgs particles could give rise to significant gamma ray lines [15]. In [14–16, 28, 30], the prospects for direct and the indirect detection of dark matter were considered. Constraints from LEP II data were derived in [17], whereas prospects for detection at colliders were analyzed in [34–36]. Recently, it was demonstrated that dark matter annihilation into the three-body final state WW^* plays a crucial role in this regime, modifying in a significant way the viable parameter space of the model and the prospects for its detection [20].

Notice, in particular, that none of these known viable regions includes the mass range $M_W < M_{H^0} < 500$ GeV. It is our goal to demonstrate that the lower part of that range, up to about 160 GeV, is another viable region of the inert doublet model. Along this new viable region, cancellations between the different diagrams that contribute to dark matter annihilation into gauge bosons are required to satisfy the relic density constraint.

4 Cancellations in the $M_{H^0} > M_W$ regime

4.1 Analytical Results

Above the W threshold, $M_{H^0} > M_W$, dark matter annihilation into W^+W^- becomes kinematically allowed, with the result that the total annihilation cross section tends to be rather large. If we estimate it from the pure gauge diagram –figure 1, (a)–, we get that

$$\sigma v_{WW}^{(s\text{-wave})} = \frac{g^4}{128\pi M_{H^0}^3} \sqrt{M_{H^0}^2 - M_W^2} \left(3 + \frac{4M_{H^0}^2(M_{H^0}^2 - M_W^2)}{M_W^4} \right), \quad (14)$$

which, for $M_{H^0} \sim 100$ GeV, gives about $2 \times 10^{-24} \text{cm}^3/\text{s}$. And a similar number is found for the annihilation into Z^0Z^0 . These annihilation cross sections are both much larger than those required to obtain the correct relic density ($\sigma v \sim 3 \times 10^{-26} \text{cm}^3/\text{s}$), so it seems difficult to satisfy the dark matter constraint in this mass range. In fact, previous analysis have claimed that it is not possible to do so. In [13], they stated that the inert Higgs could only provide a subdominant

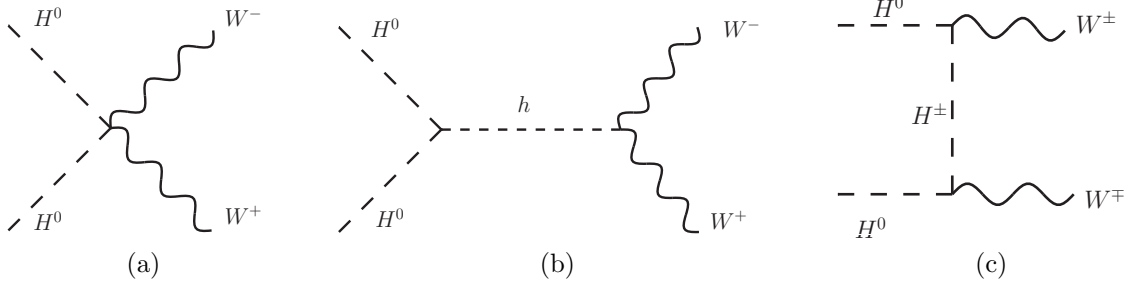


Figure 1: Feynman diagrams contributing to dark matter annihilation into W^+W^- in the inert doublet model. The exchange diagram obtained from (c) is not shown. Analogous diagrams, with W^\pm replaced by Z^0 and H^\pm by A^0 , contribute to the annihilation into Z^0Z^0 .

component of the dark matter, while in [14] they found the relic density to be too suppressed to be consistent with WMAP unless $M_{H^0} > 600$ GeV.

Here, we show that those conclusions are incorrect. Taking advantage of the interference among the different diagrams that contribute to dark matter annihilation into gauge bosons, it is possible to satisfy the relic density constraint for $M_{H^0} \gtrsim M_W$. Thus, opening up a new viable region of the inert doublet model.

Let us now explain how these interference effects come about. The diagrams that contribute to dark matter annihilation into W^+W^- (or Z^0Z^0) are shown in figure 1. Their amplitudes are given by

$$i\mathcal{M}_p = i\frac{g_V^2}{2}\epsilon_\mu^*(p_3)\epsilon^{*\mu}(p_4) \quad (15)$$

$$i\mathcal{M}_s = i\frac{\lambda_L v^2 g_V^2}{s - M_h^2 - iM_h\Gamma_h}\epsilon_\mu^*(p_3)\epsilon^{*\mu}(p_4) \quad (16)$$

$$i\mathcal{M}_t = i\frac{g_V^2}{t - M_\chi^2}p_1^\mu\epsilon_\mu^*(p_3)p_2^\nu\epsilon_\nu^*(p_4) \quad (17)$$

$$i\mathcal{M}_u = i\frac{g_V^2}{u - M_\chi^2}p_2^\mu\epsilon_\mu^*(p_3)p_1^\nu\epsilon_\nu^*(p_4) \quad (18)$$

where $\epsilon_\mu^*(p)$ is the polarization vector of the gauge boson with momentum p , p_1 and p_2 are the momenta of the H^0 's, and s , t and u are the Mandelstam variables. In these equations, $g_V = g, g/\cos\theta_W$ and $\chi = H^\pm, A^0$ respectively for the annihilations into $V = W^\pm, Z^0$. Typically, the first two contributions (the point-like interaction and the Higgs-mediated diagram) dominate the total annihilation cross section, so we will focus on those in our analytical discussion. Far from the Higgs resonance, their squared amplitude can be written as

$$|i\mathcal{M}_p + i\mathcal{M}_s|^2 = \frac{g_V^4}{4} \left(2 - \frac{1}{4} \left(\frac{s - 2M_V^2}{M_V^2} \right)^2 \right) \frac{[(s - M_h^2) + 2\lambda_L v^2]^2}{(s - M_h^2)^2}. \quad (19)$$

Since $s \simeq 4M_{H^0}^2$ at low velocities, a cancellation between the two contributions occurs for

$$\lambda_L \approx -2(M_{H^0}^2 - (M_h/2)^2)/v^2, \quad (20)$$

to which we refer as the cancellation condition. Hence, cancellations take place for $\lambda_L > 0$ if $M_{H^0} < M_h/2$ and for $\lambda_L < 0$ if $M_{H^0} > M_h/2$. For example, in the case of $M_{H^0} = 120$ GeV and $M_{H^0} < M_h/2$, cancellations occur for $\lambda_L \simeq (0.04, 0.5, 1.2, 2.0)$ when $M_h = (250, 350, 450, 550)$ respectively, while for $M_{H^0} > M_h/2$, cancellations should occur for $\lambda_L \sim [-0.35, -0.1]$ when $M_h \in [121, 200]$. Notice also, that the cancellation condition is the same for both final states, W^+W^- and Z^0Z^0 , indicating that both processes will be simultaneously suppressed. The idea, then, is that in regions of the parameter space where the cancellation condition is satisfied, the annihilation rate could be much smaller and, accordingly, a larger relic density will be found. Perhaps, large enough to be compatible with WMAP.

The existence of cancellations in the annihilation cross section into gauge bosons had already been noticed in [17] and in [20]. But the possibility of using them to obtain viable models above M_W had not been considered before.

Let us also emphasize that the t - and u -channels that we have neglected in the above analysis will certainly affect the annihilation cross section into W^+W^- and Z^0Z^0 . We will see that in order to comply with the relic density constraint it is necessary to suppress their contributions by considering large values of M_{A_0} and M_{H^\pm} .

Suppressing the annihilations into W^+W^- and Z^0Z^0 is not enough to ensure a small dark matter annihilation cross section. In addition, we must make sure that the other relevant annihilation final states, that is hh and $t\bar{t}$, do not give a large contribution to it. If $M_{H^0} > M_h$, the total s-wave contribution to the $H_0H_0 \rightarrow hh$ annihilation process is given by

$$\sigma v_{hh}^{(s\text{-wave})} = \frac{\lambda_L^2}{4\pi M_{H^0}^3} \sqrt{M_{H^0}^2 - M_h^2} \frac{(M_h^4 - 4M_{H^0}^4 - 2M_h^2 v^2 \lambda_L + 8M_{H^0}^2 v^2 \lambda_L)^2}{(M_h^4 - 6M_h^2 M_{H^0}^2 + 8M_{H^0}^4)^2}. \quad (21)$$

Using $M_{H^0} \gtrsim M_h$ and the λ_L of equation (20), we obtain that $\sigma v_{hh}^{(s\text{-wave})}$ is typically of $\mathcal{O}(10^{-23})\text{cm}^3/\text{s}$, giving rise to a very suppressed relic abundance. To be compatible with the observed dark matter density, then, the mass of the dark matter particle must be smaller than the Higgs mass ($M_{H^0} < M_h$), so that the annihilation channel into hh is not kinematically allowed. This limitation of the parameter space is not that strong in the inert doublet model, for the Higgs mass can be quite large. A very stringent constraint comes instead from the annihilation into $t\bar{t}$. The total s-wave contribution to the $H_0H_0 \rightarrow t\bar{t}$ process is given by

$$\sigma v_{t\bar{t}}^{(s\text{-wave})} = \frac{N_c \lambda_L^2 m_t^2 (M_{H^0}^2 - m_t^2)^{3/2}}{M_{H^0}^3 \pi (4M_{H^0}^2 - M_h^2)}, \quad (22)$$

where m_t is the top mass and $N_c = 3$ is the color factor. Again we find that the λ_L satisfying the cancellation condition yields a very small relic abundance for $M_{H^0} \gtrsim m_t$. Therefore, viable models must feature $M_{H^0} < m_t$. In [33], for instance, it was assumed that $M_{H^0} \gg m_t, M_h$, so the effect of cancellations was overlooked in their study. As a result, the minimal value of M_{H^0} consistent with WMAP was found to be 535 GeV. From our analysis of the mass range $M_W < M_{H^0} < 500$ GeV, we conclude that models satisfying the relic density constraint could be found only along the lower part of it, specifically for $M_{H^0} < m_t, M_h$.

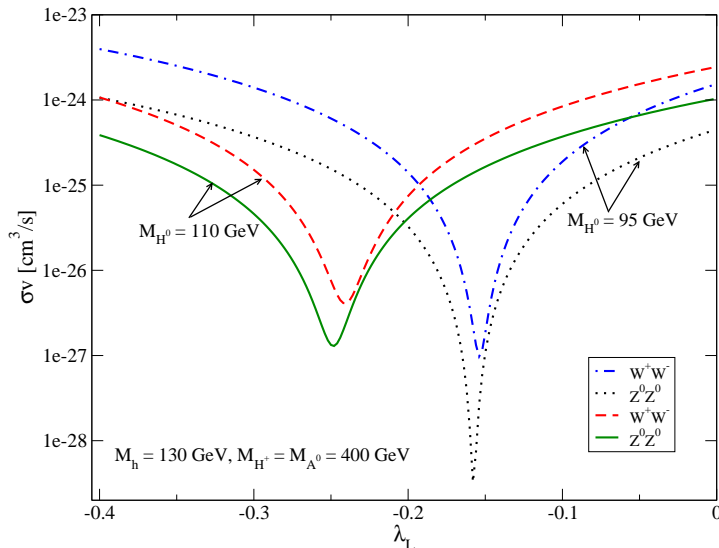


Figure 2: The dark matter annihilation cross section (at low velocity) into W^+W^- and Z^0Z^0 as a function of λ_L for two different values of M_{H^0} : 95 GeV and 110 GeV. In this figure $M_{A^0} = M_{H^\pm} = 400$ GeV and $M_h = 130$ GeV. Notice that cancellations take place simultaneously in both channels, W^+W^- and Z^0Z^0 .

When evaluating numerically the annihilation cross sections and the relic density, we always take into account all the relevant processes, and all the diagrams that contribute to a given process. The analytical expressions derived in this section are not used for that purpose. We will verify, nevertheless, that the viable models always satisfy the cancellation condition we have obtained.

These cancellation effects we have described are illustrated in figure 2, which shows the dark matter annihilation cross sections into W^+W^- and Z^0Z^0 as a function of λ_L . For this figure we set $M_h = 130$ GeV, $M_{H^\pm} = M_{A^0} = 400$ GeV, and we consider two different values of M_{H^0} : 95 GeV and 110 GeV. Equation (20) tell us that the cancellations should take place for for negative values of $\lambda_L = -0.16$ and -0.26 respectively which is in good agreement with the full numerical treatment of the annihilation cross section. We observe that the larger M_{H^0} the larger the value of $|\lambda_L|$ required to obtain cancellations. Notice from the figure that cancellations may in fact reduce significantly the annihilation cross section and that this reduction takes place simultaneously in both channels, W^+W^- and Z^0Z^0 .

Since $\Omega h^2 \propto 1/\sigma v$, we expect these cancellations in the annihilation cross section to increase significantly the inert Higgs relic density, opening up the possibility of finding viable models for $M_{H^0} \gtrsim M_W$. Next, we study, with several examples, the dependence of the relic density on the parameters of the models and show that there are indeed viable models in this region of the parameter space.

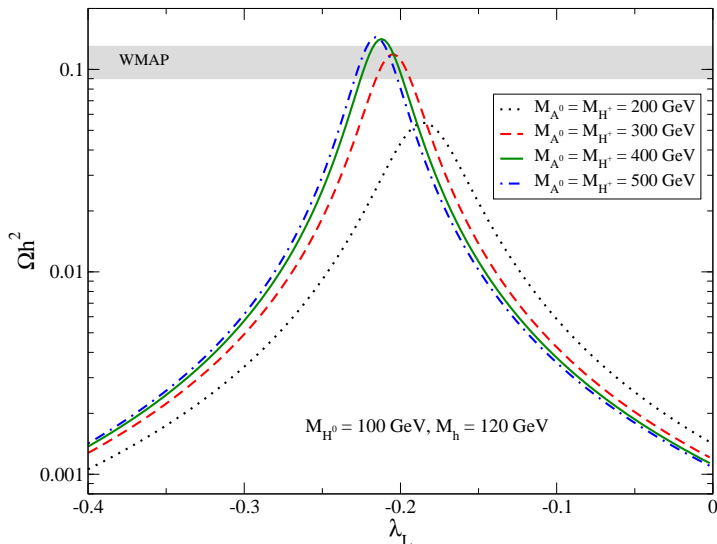


Figure 3: The relic density as a function of λ_L for several values of $M_{A^0} = M_{H^\pm}$: 200, 300, 400, 500 GeV. In this figure $M_{H^0} = 100$ GeV and $M_h = 120$ GeV.

4.2 Examples

Figure 3 shows the relic density as a function of λ_L for $M_{H^0} = 100$ GeV, $M_h = 120$ GeV and different values of M_{A^0} and M_{H^\pm} . For simplicity we consider models with $M_{A^0} = M_{H^\pm}$ and we let them vary between 200 GeV and 500 GeV. The horizontal band shows the region compatible with the observed dark matter density, $0.09 < \Omega h^2 < 0.13$. The effect of cancellations on the relic density is apparent in this figure. They increase Ωh^2 significantly as λ_L approaches about -0.2 , where the relic density reaches its maximum value. This value depends slightly on the value of $M_{A^0} = M_{H^\pm}$ but is in any case close to 0.1. Far from this maximum, say for $\lambda_L = -0.4$ or $\lambda_L = 0$, the relic density is two orders of magnitude smaller. From this figure we also learn that cancellations are necessary but not sufficient to ensure a relic density compatible with the observations. In addition, the mass of the charged scalar (and of the CP-odd scalar) should be large enough to suppress the H^\pm (and A^0) mediated contributions. If, for instance, $M_{H^\pm} \lesssim 200$ GeV cancellations are still present but the relic density is always below the observed range. For the other values of M_{H^\pm} we consider, 300, 400, 500 GeV, it is always possible to satisfy the dark matter constraint for a certain range of λ_L . And the allowed values of λ_L depend only slightly on the precise value of $M_{H^\pm} = M_{A^0}$. This first example demonstrates that in the inert doublet model it is indeed possible to satisfy the relic density constraint for $M_{H^0} \gtrsim M_W$.

The dependence of the relic density on M_{H^0} and M_h is shown in figure 4. They both display the relic density as a function of λ_L for $M_{A^0} = M_{H^\pm} = 400$ GeV. In (a), M_{H^0} was set to 100 GeV and four different values of M_h (120, 130, 140, 150 GeV) were considered. As before, the horizontal band shows the region compatible with the observed dark matter density. The effect of cancellations are evident: they allow to satisfy the dark matter bound for λ_L approximately between -0.15 (for $M_h = 150$ GeV) and -0.22 (for $M_h = 120$ GeV). As expected from equation

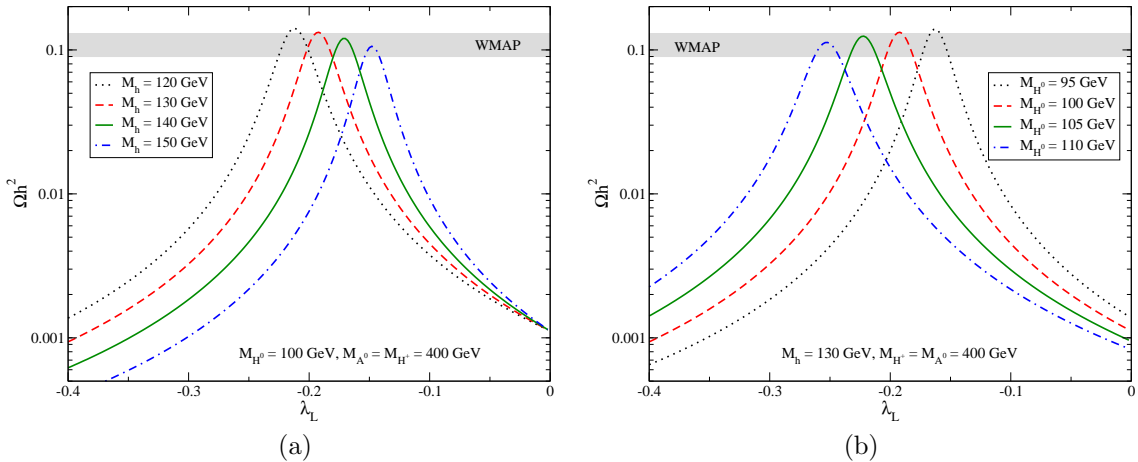


Figure 4: (a) The relic density as a function of λ_L for different values of M_h . For this figure we set $M_{H^0} = 100$ GeV and $M_{A^0} = M_{H^\pm} = 400$ GeV. (b) The relic density as a function of λ_L for different values of M_{H^0} . The other parameters were taken as $M_h = 130$ GeV and $M_{A^0} = M_{H^\pm} = 400$ GeV.

(20), the value of λ_L that gives the maximum relic density moves toward less negative values as M_h is increased. Because the Higgs-mediated contribution to dark matter annihilation is proportional to λ_L , the Higgs-dependence of the relic density disappears for $\lambda_L = 0$, as observed in the figure. At that point, the relic density is driven by the direct annihilation into gauge bosons (figure 1,(a)) resulting in $\Omega h^2 \sim 10^{-3}$. We can conclude from this figure that for $M_{H^0} = 100$ GeV and $M_{A^0} = M_{H^\pm} = 400$ GeV there is a significant range of Higgs masses for which the relic density can be consistent with the observations.

In figure 4 (b) M_h was set to 130 GeV and four different values of M_{H^0} (95, 100, 105, 110 GeV) were considered. We see that the position of the peak moves toward more negative values of λ_L as M_{H^0} is increased, in agreement with the results found previously. To obtain the observed relic density, values of λ_L approximately between -0.15 (for $M_{H^0} = 95$ GeV) and -0.27 (for $M_{H^0} = 110$ GeV) are required. These figures illustrate that the new viable region occupies a non-negligible volume in the parameter space of the inert doublet model, spanning a significant range in M_{H^0} , λ_L , M_h , M_{A^0} and M_{H^\pm} .

So far we have illustrated the effect of cancellations on the relic density only for the light Higgs regime, $M_h \lesssim 200$ GeV. A remarkable feature of the inert doublet model is that it allows for a much heavier Higgs without contradicting electroweak precision data. As we will see, cancellations leading to viable models with $M_{H^0} \gtrsim M_W$ can also take place in the heavy Higgs regime of the model, that is for $M_h > 200$ GeV.

Figure 5 is analogous to figure 4 but for a heavy Higgs boson, $M_h \sim 400$ GeV. In both panels M_{H^\pm} was set to 500 GeV and M_{A^0} to 450 GeV (they must now give a positive contribution to ΔT). In (a) the relic density is shown as a function of λ_L for $M_{H^0} = 120$ GeV and four different values of M_h : 360, 380, 400, 420 GeV. First of all, notice that in this case cancellations occur for positive rather than negative values of λ_L . As expected from the cancellation condition, the position of the

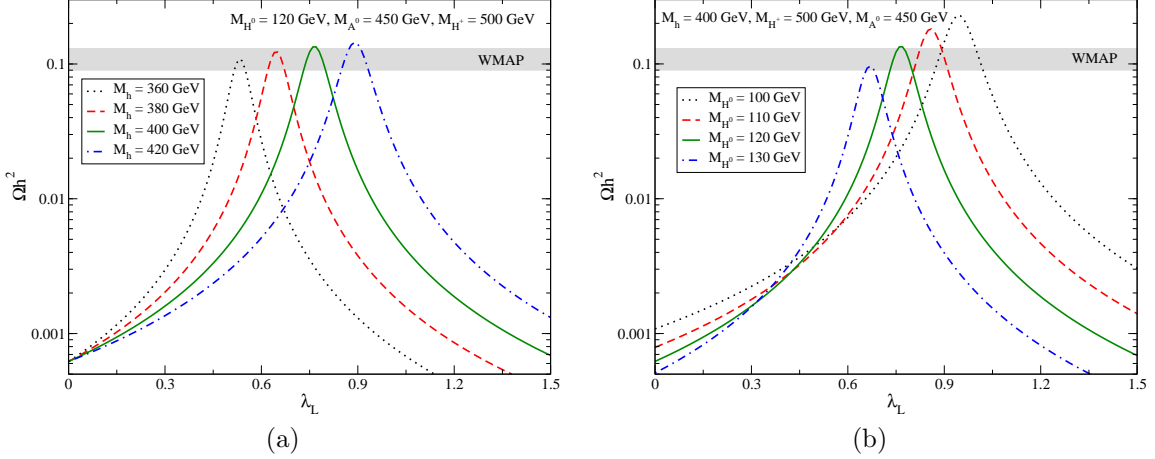


Figure 5: (a) The relic density as a function of λ_L for several Higgs masses. In this figure we set $M_{H^0} = 120$ GeV, $M_{A^0} = 450$ GeV and $M_{H^\pm} = 500$ GeV. (b) The relic density as a function of λ_L for different values of M_{H^0} : 100, 110, 120, 130 GeV. The other parameters were taken as $M_h = 400$ GeV, $M_{A^0} = 450$ GeV and $M_{H^\pm} = 500$ GeV.

peak moves toward larger values of λ_L as M_h is increased. The values of λ_L that give the correct relic density are between 0.5 (for $M_h = 360$ GeV) and about 0.9 (for $M_h = 420$ GeV). For $\lambda_L = 0$, Ωh^2 becomes independent of M_h , with a value of about 6×10^{-4} . In (b) the relic density is shown as a function of λ_L for $M_h = 400$ GeV and four different values of M_{H^0} : 100, 110, 120, 130 GeV. The viable region corresponds in this case to λ_L between 0.7 (for $M_{H^0} = 130$ GeV) and 1.0 (for $M_{H^0} = 100$ GeV). We observe that the maximum value of Ωh^2 increases as M_{H^0} is decreased. In fact, if $M_{H^0} = 130$ GeV the maximum relic density is as large as the WMAP lower limit. So, it is not possible to satisfy the relic density constraint (keeping the other parameters fixed) for $M_{H^0} > 130$ GeV. But if $M_{H^0} = 100$ GeV the relic density can be larger than the WMAP upper limit, reaching about 0.23. As a result, it is easier to satisfy the relic density constraint with a lighter inert Higgs.

As we have seen in the previous figures, cancellations between the different diagrams that contribute to dark matter annihilation into gauge bosons indeed allow to satisfy the relic density constraint for inert Higgs masses above M_W (and below m_t). In other words, there certainly exist regions in the viable parameter space of the inert doublet model that had not been considered before. What we are lacking at this point is a more complete characterization of this new viable region. We would like to know, for instance, what is the largest dark matter mass (M_{H^0}) that is allowed, what are the typical values of λ_L , M_h , M_{H^\pm} and M_{A^0} , or what is the most promising strategy to detect the inert Higgs along this region. In the next sections we will address precisely these issues.

5 The new viable region

So far, we have demonstrated the existence of a new viable region in the inert doublet model. This previously overlooked region features dark matter masses larger than M_W and is consistent with the relic density constraint thanks to cancellations between the Higgs mediated diagram and the direct annihilation diagrams into W^+W^- and Z^0Z^0 . In this section we perform a systematic analysis of this new viable region of the parameter space. To that end, we make use of Markov Chain Monte Carlo (MCMC) techniques to efficiently explore the full parameter space of the inert doublet model and find a large number of viable models in the region of interest to us. Then, we proceed to analyze such models in detail.

5.1 The scan

The inert doublet model contains 5 free parameters that can be taken to be M_{H^0} , M_{H^\pm} , M_{A^0} , λ_L , and M_h . We allow these parameters to vary within the following ranges:

$$80 \text{ GeV} < M_{H^0} < 200 \text{ GeV} \quad (23)$$

$$80 \text{ GeV} < M_{H^\pm} < 1000 \text{ GeV} \quad (24)$$

$$80 \text{ GeV} < M_{A^0} < 1000 \text{ GeV} \quad (25)$$

$$-12 < \lambda_L < 12 \quad (26)$$

$$114 \text{ GeV} < M_h < 600 \text{ GeV} \quad (27)$$

MCMC techniques allow us to scan freely and efficiently over these 5 parameters. Let us emphasize that these techniques have already been successfully used to scan and analyze the viable parameter space of other models of dark matter, see [38, 39]. Here we closely follow the procedure outlined in [38].

After scanning the above parameter space, we get a large sample of viable models, satisfying all the experimental and theoretical bounds and the relic density constraint. For our analysis we generated about 40000 such models within the new viable region. In the remaining part of the paper, we will work exclusively with this sample of models, analyzing its main features and studying its implications.

5.2 Different projections of the viable region

To facilitate the analysis and visualization of the 5-dimensional region where the viable models are located, we will project it onto different two-dimensional planes. Figure 6, for instance, shows the new viable region of the inert doublet model in the plane (M_{H^0}, λ_L) . To generate this kind of figures, we created a suitable grid in the two variables (M_{H^0} and λ_L in this case) and we place a point at a given value of them if there is at least one viable model in our sample with such coordinates. Sometimes we also differentiate (using symbols and colours) various ranges for other important parameters (the Higgs mass in figure 6) that may provide additional information. Notice in figure 6 that the value of M_{H^0} over the new region extends from M_W up to about 160 GeV. We argued in section 4 that M_{H^0} had to be smaller than $m_t = 171.4$ GeV but at that point we did not know how close to m_t it could get. In λ_L , the range of possible values extends from -0.5 to about 3.0 . A sharp contrast is observed between the models with $\lambda_L < 0$ and those with $\lambda_L > 0$. In the former case ($\lambda_L < 0$), the maximum value of M_{H^0} is about 130 GeV and the

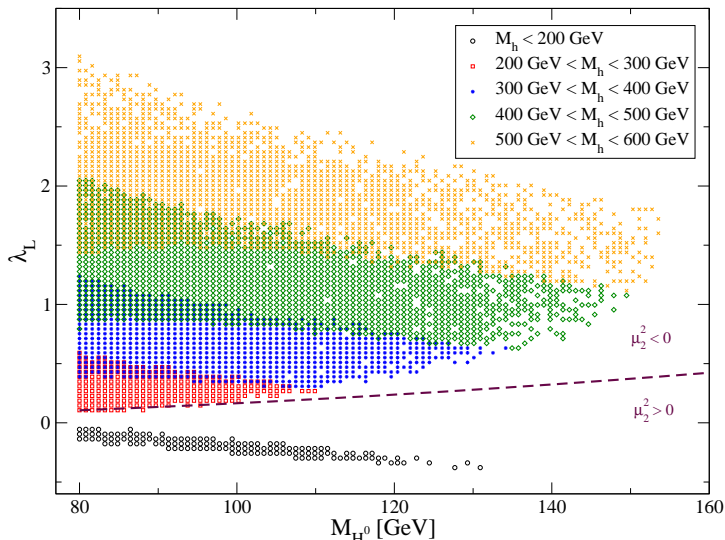


Figure 6: The new viable region projected on the plane (M_{H^0}, λ_L) . The different symbols (and colors) distinguish among the possible ranges of M_h . The dashed line is the contour $\mu_2^2 = 0$. Above that line μ_2^2 is negative whereas it is positive below it.

Higgs boson is necessarily light, $M_h < 200$ GeV, as cancellations occur for $M_{H^0} > M_h/2$. In the latter case ($\lambda_L > 0$), the maximum value of M_{H^0} can be larger, strongly depending on the range of Higgs masses. Thus, for $200 \text{ GeV} < M_h < 300 \text{ GeV}$ the maximum M_{H^0} is only about 110 GeV whereas it can reach almost 160 GeV for the largest Higgs masses, $M_h > 500$ GeV. It is also apparent from the figure, that for $\lambda_L > 0$ the larger the Higgs mass the larger λ_L must be. Given that cancellations are needed to obtain the correct relic density, it is not surprising that no viable models are found with λ_L close to zero, as in that region the Higgs-mediated diagram becomes negligible. Finally, the dashed line shows the contour $\mu_2^2 = 0$. From the figure we see that viable points with $\mu_2^2 > 0$ feature $\lambda_L < 0$ and viceversa.

The dependence of the new viable region on M_{H^\pm} and M_{A^0} is illustrated in figure 7. Panel (a) shows the projection on the plane (M_{H^0}, M_{H^\pm}) for different ranges of M_{A^0} . The trend is clear: the heavier the dark matter particle the larger M_{H^\pm} must be. If $M_{H^0} < 100$ GeV, M_{H^\pm} can take values within a wide range, but as M_{H^0} increases, higher and higher values of M_{H^\pm} are required. If, for instance, $M_{H^0} > 130$ GeV, M_{H^\pm} should be larger than about 400 GeV. And the viable models with the highest dark matter masses ($M_{H^0} > 150$ GeV) all feature a heavy H^\pm (and a heavy A^0), $M_{H^\pm} > 500$ GeV. It is also observed in the figure that there is a correlation between the values of M_{H^\pm} and M_{A^0} . Large values of M_{H^\pm} are associated with large values of M_{A^0} . This correlation is illustrated in more detail in panel (b) of the same figure, which shows the viable region in the plane (M_{A^0}, M_{H^\pm}) for different ranges of the Higgs mass. In this plane, the viable models are concentrated along a band just above the $M_{H^\pm} = M_{A^0}$ line (the diagonal). In other words, most models feature $M_{H^\pm} > M_{A^0}$ but their mass splitting is never that large. Let us emphasize that this condition is not enforced by the dark matter constraint but rather by

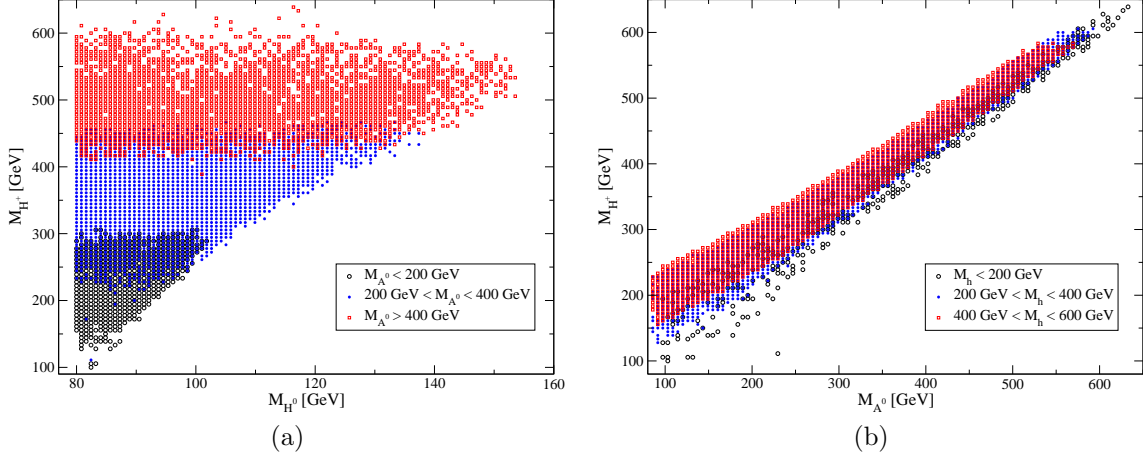


Figure 7: (a) The new viable region projected on the plane (M_{H^0}, M_{H^\pm}) . Different symbols (and colors) are used to distinguish the possible values of M_{A^0} . (b) The new viable region projected on the plane (M_{A^0}, M_{H^\pm}) . Three possible ranges of M_h are set apart with different symbols (and colors).

electroweak precision data, see equations (9) and (12). We see then that both M_{A^0} and M_{H^\pm} can be as large as 650 GeV and that the models with the highest dark matter masses ($M_{H^0} \gtrsim 140$ GeV) require them to be larger than about 500 GeV.

In figure 8 we show the new viable region in the plane (M_{H^0}, M_h) . The Higgs resonance line, $2M_{H^0} = M_h$, is also shown for illustration. A priori we do not expect to find viable models close to that line, for resonant annihilations would drive the relic density to very small values. Points lying below the Higgs resonance line correspond to models with $2M_{H^0} > M_h$ and they all feature $\lambda_L < 0$. From the figure we see that such points extend up to about 130 GeV in M_{H^0} and about 160 GeV in M_h . They correspond, therefore, to what we call the light Higgs regime. Points above the Higgs resonance line ($2M_{H^0} < M_h$), in contrast, all feature a positive value of λ_L . It can be observed that they include dark matter masses as high as 160 GeV and Higgs bosons heavier than 200 GeV and extending up to 600 GeV. Hence, they lie within the heavy Higgs regime. Finally it is worth mentioning that no viable models are found for Higgs masses approximately between 160 GeV and 200 GeV.

We have in this way determined the position of the new viable region in the 5-dimensional space formed by M_{H^0} , M_{A^0} , M_{H^\pm} , λ_L and M_h . It is also useful to understand its position in the space of λ parameters, which consists of λ_3 , λ_4 and λ_5 . The reason is that some constraints, such as the perturbativity and the vacuum stability bounds, are applied directly to these couplings, not to scalar masses or to λ_L . Since many models feature a rather heavy H^\pm and μ_2^2 negative (equivalently λ_L positive), we expect that a larger value of λ_3 will be required –see equation (2). That is what we observed in figure 9. It displays the new viable region in the plane (M_{H^0}, λ_3) for different ranges of M_h . We see that λ_3 can indeed be large, with some models lying right at the perturbativity limit, $\lambda_3 = 4\pi$ (dotted line). In the figure we observe that the models with the largest dark matter masses ($M_{H^0} \gtrsim 140$ GeV), in particular, feature $\lambda_3 \gtrsim 9$. It must be

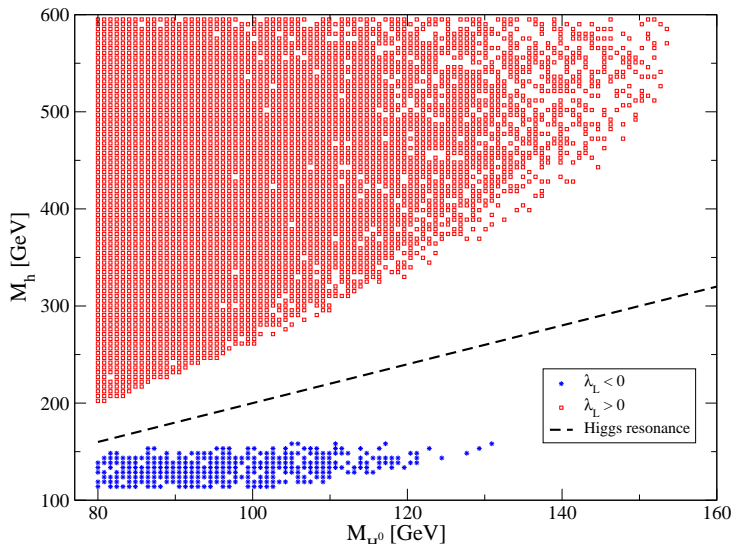


Figure 8: The new viable region projected on the plane (M_{H^0}, M_h) . The line shows the position of the Higgs resonance region, $2M_{H^0} = M_h$. Different colors and symbols are used to differentiate models with $\lambda_L > 0$ from those with $\lambda_L < 0$.

emphasized, however, that λ_3 is not that large over the entire new viable region. Models with $\lambda_3 < 6$, for instance, extend up to $M_{H^0} = 120$ GeV while those with $\lambda_3 \lesssim 2$ can reach up to 105 GeV. Thus, if one wants to impose a more restrictive perturbativity bound on λ_3 , this figure can be used to find out the resulting viable range of M_{H^0} .

Figure 10 shows the new viable regions in the planes (M_{H^0}, λ_4) and (M_{H^0}, λ_5) . λ_4 turns out to be negative in most models and reaches at most $|\lambda_4| = 7$, significantly below the perturbativity limit (not shown). The possible values of λ_4 move toward lower values as M_{H^0} is increased. Hence, for $M_{H^0} = 100$ GeV $\lambda_4 \in (-1, -7)$ whereas for $M_{H^0} = 130$ GeV $\lambda_4 \in (-3, -7)$. Notice also that $\lambda_4 \sim -5$ for the models with the largest values of M_{H^0} . λ_5 , which determines the mass splitting between H^0 and A^0 , is by definition negative ($M_{A^0} > M_{H^0}$). We see, in panel (b), that its absolute value is never larger than 7 and only rarely exceeds 5, placing it comfortably within the perturbative regime. As with λ_4 , the allowed values of λ_5 tend to move toward lower values (higher $|\lambda_5|$) as M_{H^0} is increased. For the models with the highest dark matter masses, λ_5 is about -4.0 . Consequently, a more restrictive perturbativity bound on λ_4 and λ_5 , say $\lambda_{4,5} < 5$, could be imposed without affecting the viable range of M_{H^0} .

We thus conclude this subsection regarding the projections of the viable region onto different two-dimensional planes. Before addressing the implications of the new viable region for the direct and the indirect detection of inert Higgs dark matter, we will discuss the issue of the fine-tuning required to obtain the correct relic density within this new viable region. Is it large, moderate or small? How does it compare against the fine-tuning found in other models of dark matter?

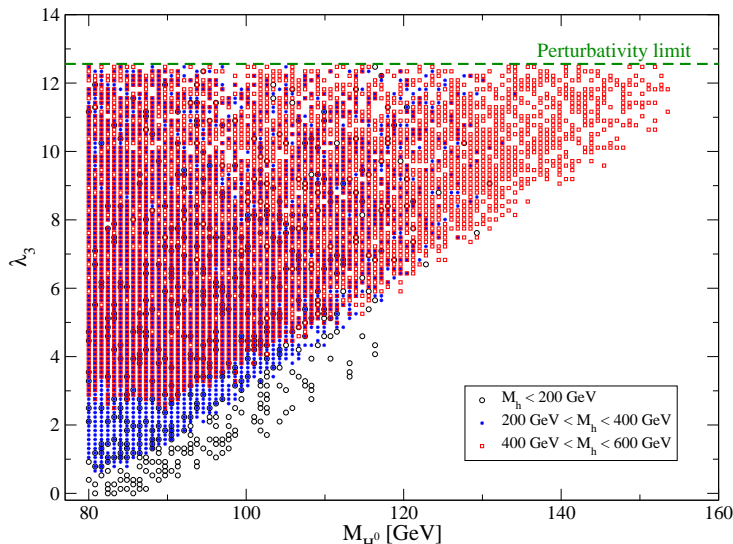


Figure 9: The new viable region projected on the plane (M_{H^0}, λ_3) . The different symbols (and colors) distinguish among the possible ranges of M_h . The dotted line shows the perturbativity limit, $\lambda_3 = 4\pi$.

5.3 Fine-tuning

Given that in it cancellations are necessary to obtain the right relic density, one may think that this new viable region of the inert doublet model is disfavoured by fine-tuning arguments. Here, we quantify the fine-tuning of the viable models and show that that is not really the case. Many of them feature low to moderate fine-tuning and none of them has a very large one.

The issue of the fine-tuning required to satisfy the dark matter constraint is not new. In [40], where this fine-tuning was first quantified, it was proposed to use as a fine-tuning parameter the logarithmic sensitivity of the relic density to variations in the input parameters of the model. If a_i ($i = 1, \dots, n$) are free parameters of a given dark matter model, the fine-tuning parameter (of the relic density) with respect to a_i , $\Delta_{\Omega h^2, a_i}$ is given by

$$\Delta_{\Omega h^2, a_i} \equiv \frac{\partial \log \Omega h^2}{\partial \log a_i}. \quad (28)$$

And the total fine-tuning, $\Delta_{\Omega h^2, \text{total}}$, is obtained by summing in quadrature the contributions of the different parameters of the model. Thus, in the inert doublet model we have that

$$\Delta_{\Omega h^2, \text{total}} = \sqrt{\Delta_{\Omega h^2, M_{H^0}}^2 + \Delta_{\Omega h^2, M_{H^\pm}}^2 + \Delta_{\Omega h^2, M_{A^0}}^2 + \Delta_{\Omega h^2, \lambda_L}^2 + \Delta_{\Omega h^2, M_h}^2}. \quad (29)$$

Hence, the fine-tuning parameter is large if a small variation in the parameters of the models leads to a large modification of the relic density. If, for instance, $\Delta_{\Omega h^2, \text{total}} \lesssim 10$, a measurement of the parameters of the model at the 10% level will enable to compute Ωh^2 to within a factor

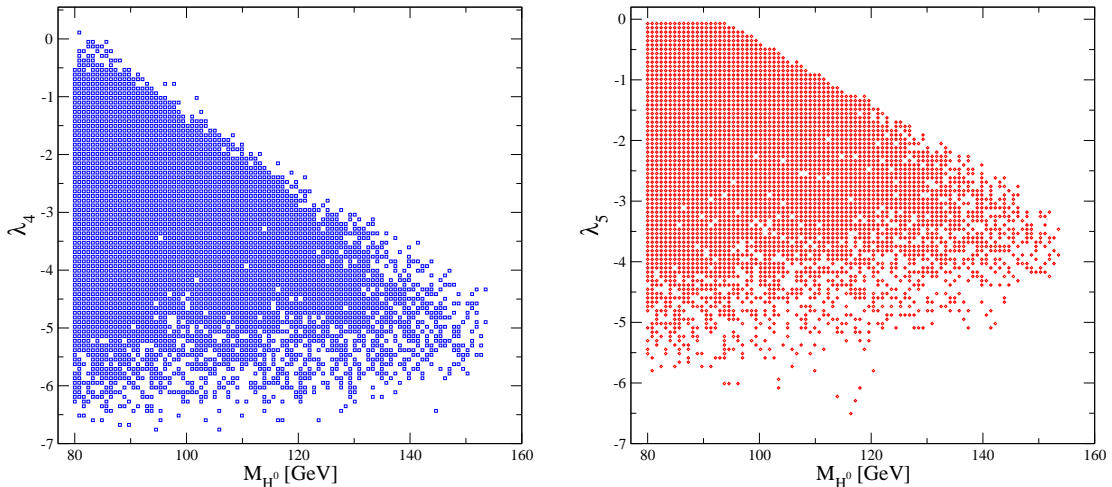


Figure 10: The new viable region projected on the planes (M_{H^0}, λ_4) (left panel) and (M_{H^0}, λ_5) (right panel).

$\mathcal{O}(2)$. As a rule of thumb, one can say that the fine-tuning is small if $\Delta_{\Omega h^2, \text{total}} \lesssim 10$, moderate for $10 < \Delta_{\Omega h^2, \text{total}} \lesssim 100$ and large if $\Delta_{\Omega h^2, \text{total}} > 100$.

Figure 11 shows the fine-tuning parameter as a function of M_{H^0} along the new viable region of the inert doublet model. $\Delta_{\Omega h^2, \text{total}}$ is typically smaller than 30, with plenty of models featuring $\Delta_{\Omega h^2, \text{total}} < 10$ over the entire range of M_{H^0} and no models with a fine-tuning parameter larger than 40. In particular, notice that there is no correlation between $\Delta_{\Omega h^2, \text{total}}$ and M_{H^0} . Low fine-tuning models, $\Delta_{\Omega h^2, \text{total}} \lesssim 10$, exist for M_{H^0} just slightly above M_W as well as for $M_{H^0} > 140$ GeV. And the same holds for moderate fine-tuning models, $\Delta_{\Omega h^2, \text{total}} \gtrsim 20$.

These results can be compared with those obtained in previous works for one of the most studied models of dark matter, the Constrained Minimal Supersymmetric Standard Model (CMSSM or mSUGRA). It turns out that the viable regions of the CMSSM tend to be highly fine-tuned, with some regions, such as the focus-point and the funnel region, featuring a $\Delta_{\Omega h^2, \text{total}}$ greater than 100 [40, 41]. In contrast, in the new viable region of the inert doublet model we are studying, the fine-tuning parameter is never that high.

6 Implications for detection

In the previous section we described in detail the new viable region of the inert doublet model. Here, we examine its implications for the detectability of the inert doublet model via collider signals and the direct and the indirect detection of inert Higgs dark matter.

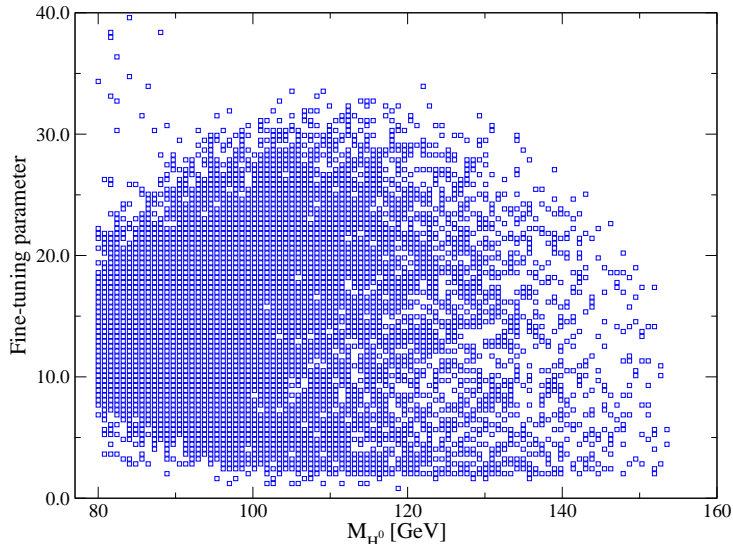


Figure 11: The fine-tuning parameter, $\Delta_{\Omega h^2, \text{total}}$, as a function of M_{H^0} along the new viable region of the model.

6.1 Collider signals

The inert doublet model can be tested at colliders via the production and decay of inert particles or through the increase in the decay width of the Higgs boson [13]. Indeed, the decay processes

$$h \rightarrow H^0 H^0, A^0 A^0, H^+ H^- \quad (30)$$

may enhance the Standard Model Higgs decay width when $M_h > 2M_{H^0}$, with important implications for Higgs searches at Tevatron and at the LHC. For the dark matter mass range we are studying, this increase is mainly due to the $H^0 H^0$ final state and it takes place only when $\lambda_L > 0$ and $M_h > 200$ GeV, see figure 6. As a consequence, the Higgs decay width considered in the recent summary of Higgs searches at Tevatron below 200 GeV [42] is left untouched by the inert scalars for $M_{H^0} > M_W$. The LHC, on the other hand, is expected to perform direct measurements of the Higgs decay width with a precision of about 6% [43] for $300 \text{ GeV} < M_h < 700 \text{ GeV}$.

Figure 12 shows the Higgs branching ratio into $H^0 H^0$ as a function of the Higgs mass for our sample of viable models. It lies approximately between 5% and 60%. In this figure, different ranges of M_{H^0} are distinguished. For models with $M_{H^0} > 140$ GeV, $\text{BR}(h \rightarrow H^0 H^0)$ is observed to be about 10% or less. Branching ratios greater than 20% or so can also be found but only for models with the smallest dark matter masses, $M_{H^0} \lesssim 100$ GeV. In such case, the inert Higgs could be within the reach of LHC via measurements of the Higgs decay width.

6.2 Indirect detection

The indirect detection signatures of dark matter are determined, on the particle physics side, by the present annihilation rate and by the annihilation branching ratios. Figure 13 shows the present

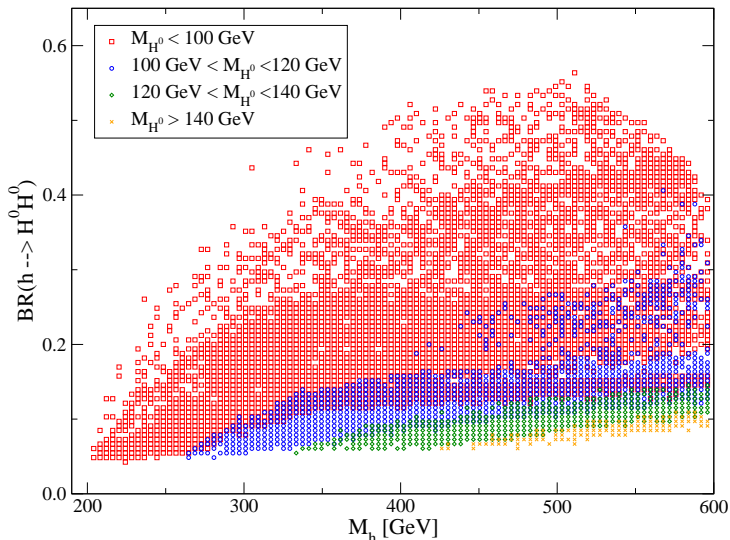


Figure 12: The decay branching ratio of the Higgs boson into the inert scalars as a function of M_h for different ranges of M_{H^0} . Only models with $\lambda_L > 0$ give a non-zero contribution to this branching.

dark matter annihilation rate, σv , as a function of M_{H^0} along the new viable region (v is taken to be 10^{-3}). We see that most points are confined within a small interval between $0.5 \times 10^{-26} \text{cm}^3/\text{s}$ and $4 \times 10^{-26} \text{cm}^3/\text{s}$. In other words, the present annihilation rate is always close to the typical value for a *thermal* relic, $\langle \sigma v \rangle \sim 3 \times 10^{-26} \text{cm}^3/\text{s}$. This outcome is a consequence of the fact that the annihilation of inert Higgs dark matter is dominated by its s-wave component, so σv remains unchanged between the early Universe and the present time. Besides, coannihilations, with A^0 or H^\pm , play no important role in the region we are considering, as they would drive the relic density to even smaller values.

In the new viable region, the inert Higgs annihilates mainly into $b\bar{b}$, W^+W^- and Z^0Z^0 (the hh and $t\bar{t}$ final states are kinematically forbidden). Figure 14 shows the annihilation branching ratio (BR) into these three final states as a function of M_{H^0} . We see, in the left panel, that the maximum value of $\text{BR}(H^0H^0 \rightarrow b\bar{b})$ decreases with M_{H^0} , going from about 0.85 for $M_{H^0} \sim 80$ GeV to about 0.2 for $M_{H^0} \sim 140$ GeV. The minimum value of $\text{BR}(H^0H^0 \rightarrow b\bar{b})$, on the other hand, tends to remain constant at about 0.15. In particular, the $b\bar{b}$ final state is never negligible within the new viable region. The center panel shows the branching ratio into W^+W^- . As M_{H^0} crosses the Z^0 threshold, the annihilation into Z^0Z^0 start playing a significant role and the branching into W^+W^- is therefore reduced. It is also observed in figure 14 that the range of variation of $\text{BR}(H^0H^0 \rightarrow W^+W^-)$ shrinks as M_{H^0} increases. For $M_{H^0} > 120$ GeV $\text{BR}(H^0H^0 \rightarrow W^+W^-)$ lies approximately between 0.3 and 0.5. Finally, the right panel shows $\text{BR}(H^0H^0 \rightarrow Z^0Z^0)$. It never exceeds 40%, reaching values between 0.25 and 0.35 for $M_{H^0} > 120$ GeV, and lower values for smaller M_{H^0} . Comparing the three panels we can deduce that $b\bar{b}$, W^+W^- and Z^0Z^0 are indeed the dominant annihilation channels, as their combined branching is always close to 100%.

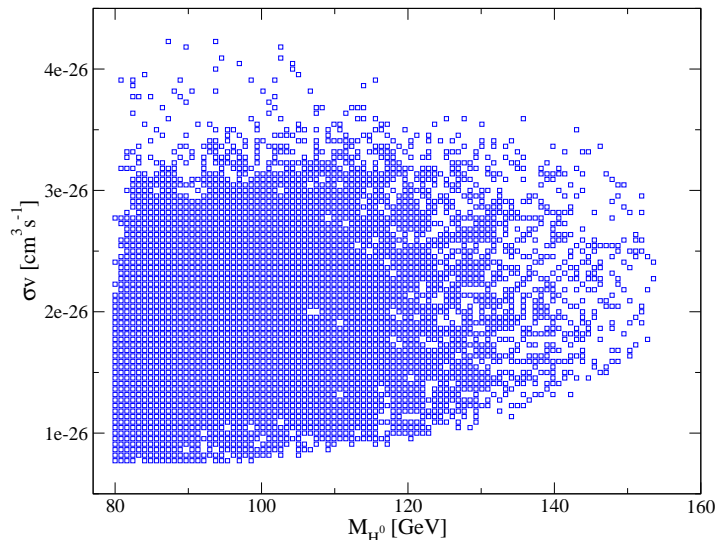


Figure 13: The present dark matter annihilation rate, σv , as a function of M_{H^0} along the new viable region of the model. Notice that σv varies only over a small range, approximately between 1×10^{-26} and $4 \times 10^{-26} \text{cm}^3/\text{s}$.

The remaining annihilation channels, into light fermions, typically account for less than 10% of the annihilations.

The present annihilation rate and the branching ratios that we have calculated determine the indirect detection signatures of inert Higgs dark matter. To illustrate the prospects for the indirect detection of dark matter along this new viable region, we compute the expected gamma ray flux from the annihilation of inert Higgs particles and compare it with present data from FERMI.

The gamma ray flux from dark matter annihilations originating in a region $\Delta\Omega$ of the sky can be written as

$$\frac{d\Phi_{\text{halo}}}{dE} = \frac{1}{2} \frac{\sigma v}{4\pi} r_{\odot} \frac{\rho_{\odot}^2}{m_{\text{DM}}^2} \bar{J} \Delta\Omega \frac{dN}{dE}, \quad (31)$$

where $r_{\odot} = 8.5$ kpc is the distance from the Sun to the Galactic Center, $\rho_{\odot} = 0.39 \text{ GeV}/\text{cm}^3$ is the local density of dark matter [44], dN/dE is the photon spectrum, and $\bar{J} \Delta\Omega$ is given by

$$\bar{J} \Delta\Omega = \int_{\Delta\Omega} d\Omega(b, l) \int_{\text{los}} \frac{ds}{r_{\odot}} \left(\frac{\rho_{\text{halo}}(r(s, \psi))}{\rho_{\odot}} \right)^2. \quad (32)$$

For the galactic distribution of dark matter we consider a NFW profile [45],

$$\rho_{\text{NFW}}(r) = \rho_s \frac{r_s}{r} \left(1 + \frac{r}{r_s} \right)^{-2}, \quad (33)$$

where $r_s = 20$ kpc and $\rho_s = 0.34 \text{ GeV}/\text{cm}^3$. For definiteness we consider the observation region $10^\circ < |b| < 20^\circ$, for which there is available data from FERMI – see [46] and the supplementary

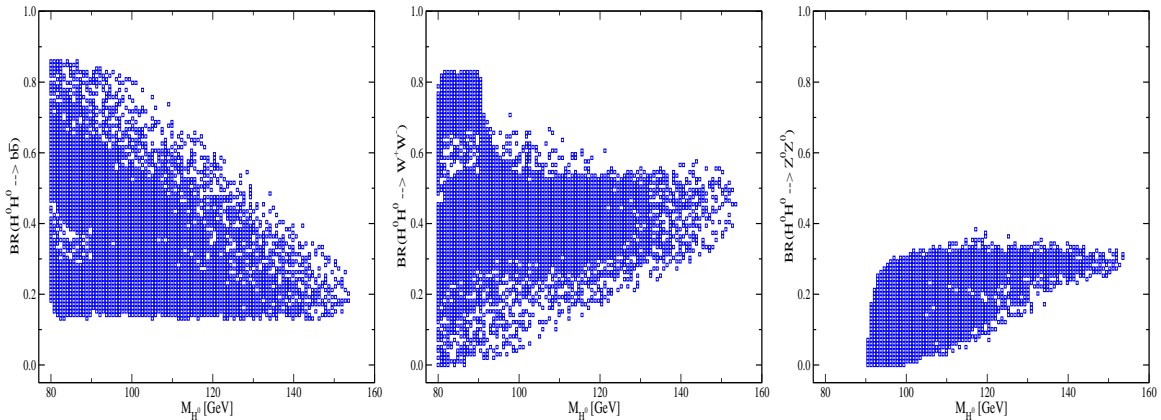


Figure 14: The main annihilation branching ratios of inert Higgs dark matter as a function of M_{H^0} . The different panels show, from left to right, $b\bar{b}$, W^+W^- , and Z^0Z^0 .

online material. The photon spectrum from dark matter annihilations, dN/dE , depends on the annihilation branching ratios and has been obtained using micrOMEGAs.

Figure 15 shows the differential gamma ray flux at 1 GeV (left panel) and at 10 GeV (right panel) for our sample of models. For $E_\gamma = 10$ GeV, it lies approximately between 5.0×10^{-6} and 2.5×10^{-5} MeV/(cm² sr), and at slightly smaller values (particularly at large masses) for 1 GeV. Unfortunately, these fluxes are much smaller than those measured by FERMI [46], which are consistent with the predictions of cosmic ray models. It is thus not possible to obtain any constraints from this data.

Let us stress that this somewhat disappointing result is consistent with previous analysis of FERMI data, see e.g. [47]. In them, it had been found that present data from FERMI can be used to rule out dark matter annihilation cross sections exceeding 10^{-23} or 10^{-24} cm³/s (depending on the dark matter mass and annihilation final state). Such cross sections are much larger than those expected in typical models of dark matter and, in particular, than those we have found along the new viable region of the inert doublet model.

6.3 Direct detection

Dark matter can also be detected via elastic scattering with terrestrial detectors, the so-called direct detection method. From a particle physics point of view, the quantity that determines the direct detection rate of a dark matter particle is the dark matter-nucleon scattering cross section. In the inert Higgs model, the H^0N scattering process relevant for direct detection is Higgs-mediated, with a cross section, σ_{H^0N} , given by

$$\sigma_{H^0N} = \frac{m_r^2}{4\pi} \left(\frac{\lambda_L}{M_{H^0} m_h^2} \right)^2 f^2 m_N^2 \quad (34)$$

where $f \sim 0.3$ is a form factor and m_r is the reduced mass of the system. Thus, it is proportional to λ_L^2 . Given the rather large values of λ_L we found, see figure 6, we foresee that σ_{H^0N} will be

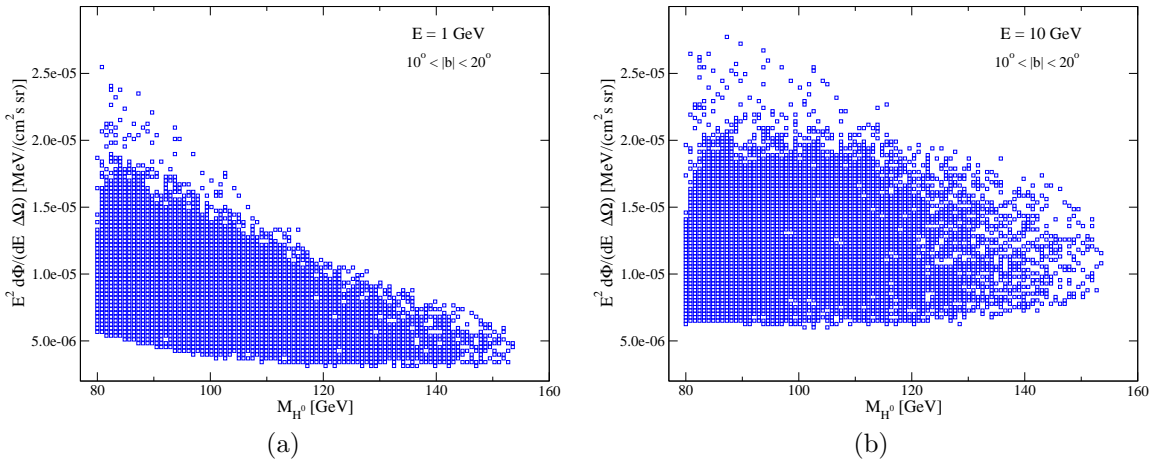


Figure 15: The expected gamma ray flux at 1 GeV (left) and 10 GeV (right) as a function of M_{H^0} for our set of viable models. The observation region is $10^\circ < |b| < 20^\circ$ in both panels.

significant over the entire new viable region. Figure 16 shows the spin-independent dark matter-nucleon cross section, $\sigma_{H^0 N}$, as a function of M_{H^0} for our sample of models. $\sigma_{H^0 N}$ lies in a narrow range between 3×10^{-7} and 10^{-8} Pb. To ease the comparison with present experimental data, the bound from the CDMS experiment [37] is also shown (as a solid line) as well as the expected sensitivity of Xenon100 (dotted line) [48]. Points lying above the CDMS line are not consistent with present bounds whereas points above the Xenon100 line are within the reach of that experiment. As observed in the figure, a non-negligible fraction of the new viable region is ruled out by direct detection constraints. In particular, most models with $M_h < 200$ GeV (though not all of them) have a direct detection cross section exceeding the CDMS bound. No range of M_{H^0} is excluded, however. The good news is that all these viable models feature cross sections close to current bounds. They are all well within the sensitivity of Xenon100. Clearly, direct detection is a promising way of probing this new viable region of the inert doublet model.

7 Conclusions

The inert doublet model is a simple and appealing extension of the Standard Model that can account for the dark matter. We have demonstrated, in this paper, the existence of a new, previously overlooked, viable region of this model featuring dark matter masses between M_W and about 160 GeV. In this region of the parameter space, the correct relic density can be obtained thanks to cancellations between the different diagrams that contribute to dark matter annihilation into gauge bosons. In the first part of the paper, we illustrated how these cancellations come about and analyzed the dependence of the annihilation cross section and the relic density on the different parameters of the model. Several examples of viable models were found both in the light Higgs regime, $M_h < 200$ GeV, and in the heavy Higgs regime, $M_h > 200$ GeV. In the second part of the paper, we made use of Markov Chain Monte Carlo techniques to obtain a large sample of

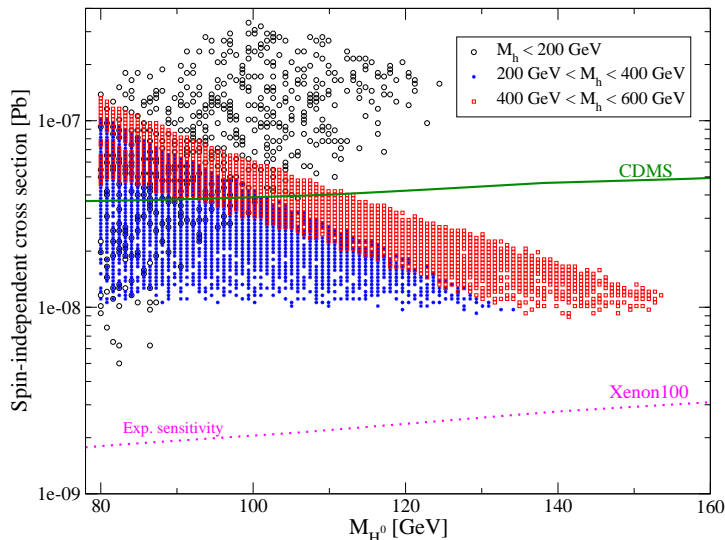


Figure 16: The spin-independent direct detection cross section as a function of M_{H^0} along the new viable region of the inert doublet model. Three possible ranges of M_h are distinguished by different symbols (and colors). The solid line shows the current bound from CDMS whereas the dotted line corresponds to the expected sensitivity of Xenon100.

models within the new viable region. These models were then analyzed in detail by projecting them onto several two-dimensional planes. From these projections we learned, for instance, that for $M_h < 200$ GeV the dark matter particle mass can be as large as 130 GeV whereas λ_L is small and negative ($0 > \lambda_L > -0.5$). Dark matter masses above 130 GeV (up to 160 GeV) can also be found but they feature heavy Higgs masses and positive values of λ_L ($3 > \lambda_L > 0$). It was also noticed that the allowed values of M_{H^\pm} and M_{A^0} increase with M_{H^0} along the new viable region, reaching $M_{A^0}, M_{H^\pm} \gtrsim 500$ GeV for $M_{H^0} \gtrsim 140$ GeV. In addition, we addressed the issue of the fine-tuning required to obtain the right relic density and showed that all these models feature a small or moderate value of the fine-tuning parameter. Finally, we considered the detection prospects of inert Higgs dark matter within the new viable region. For collider searches, the Higgs decay decay rate begins to differ from the Standard Model one for Higgs masses larger than 200 GeV. The extra contribution resulting from Higgs decays into inert scalars for $M_h > 300$ GeV might be observed directly at LHC. Regarding indirect detection, the present annihilation rate, the dominant branching fractions, and the expected gamma ray flux from dark matter annihilation were computed. But no bounds could be derived from current gamma ray data. The direct detection cross section was also calculated and found to be rather large. A fraction of the new viable parameter space, in fact, is already ruled out by present constraints from CDMS, and the remaining part will be entirely within the expected sensitivity of Xenon100. Direct detection seems to be, therefore, the most promising way of probing this new viable region of the inert doublet model.

Acknowledgments

It is a pleasure to thank M. Gustafsson, E. Nardi and M. Tytgat for comments and suggestions. L. L. H is supported in part by the IISN and by Belgian Science Policy (IAP VI/11). C. E. Y. is supported by the *Juan de la Cierva* program of the MICINN of Spain. He acknowledges additional support from the MICINN Consolider-Ingenio 2010 Programme under grant MULTIDARK CSD2009-00064, from the MCIINN under Proyecto Nacional FPA2009-08958, and from the CAM under grant HEPHACOS S2009/ESP-1473.

References

- [1] E. Komatsu *et al.* [WMAP Collaboration], *Astrophys. J. Suppl.* **180** (2009) 330 [arXiv:0803.0547 [astro-ph]].
- [2] <http://cdms.berkeley.edu/>
- [3] <http://xenon.astro.columbia.edu/>
- [4] <http://fermi.gsfc.nasa.gov>.
- [5] <http://pamela.roma2.infn.it/index.php>
- [6] <http://icecube.wisc.edu/>
- [7] H. Goldberg, *Phys. Rev. Lett.* **50**, 1419 (1983) [Erratum-*ibid.* **103**, 099905 (2009)]., J. R. Ellis, J. S. Hagelin, D. V. Nanopoulos, K. A. Olive and M. Srednicki, *Nucl. Phys. B* **238**, 453 (1984).
- [8] F. Takayama and M. Yamaguchi, *Phys. Lett. B* **485**, 388 (2000) [arXiv:hep-ph/0005214]. W. Buchmuller, L. Covi, K. Hamaguchi, A. Ibarra and T. Yanagida, *JHEP* **0703**, 037 (2007) [arXiv:hep-ph/0702184].
- [9] H. C. Cheng, J. L. Feng and K. T. Matchev, *Phys. Rev. Lett.* **89**, 211301 (2002) [arXiv:hep-ph/0207125]. G. Servant and T. M. P. Tait, *Nucl. Phys. B* **650**, 391 (2003) [arXiv:hep-ph/0206071].
- [10] J. McDonald, *Phys. Rev. D* **50** (1994) 3637 [arXiv:hep-ph/0702143]. C. P. Burgess, M. Pospelov and T. ter Veldhuis, *Nucl. Phys. B* **619** (2001) 709 [arXiv:hep-ph/0011335]. H. Davoudiasl, R. Kitano, T. Li and H. Murayama, *Phys. Lett. B* **609** (2005) 117 [arXiv:hep-ph/0405097]. V. Barger, P. Langacker, M. McCaskey, M. J. Ramsey-Musolf and G. Shaughnessy, *Phys. Rev. D* **77** (2008) 035005 [arXiv:0706.4311 [hep-ph]]. R. Dick, R. B. Mann and K. E. Wunderle, *Nucl. Phys. B* **805** (2008) 207 [arXiv:0803.1444 [astro-ph]]. C. E. Yaguna, *JCAP* **0903** (2009) 003 [arXiv:0810.4267 [hep-ph]]. A. Goudelis, Y. Mambrini and C. Yaguna, arXiv:0909.2799 [hep-ph].
- [11] N. G. Deshpande and E. Ma, *Phys. Rev. D* **18**, 2574 (1978).
- [12] E. Ma, *Phys. Rev. D* **73** (2006) 077301 [arXiv:hep-ph/0601225].

- [13] R. Barbieri, L. J. Hall and V. S. Rychkov, Phys. Rev. D **74** (2006) 015007 [arXiv:hep-ph/0603188].
- [14] L. Lopez Honorez, E. Nezri, J. F. Oliver and M. H. G. Tytgat, JCAP **0702** (2007) 028 [arXiv:hep-ph/0612275].
- [15] M. Gustafsson, E. Lundstrom, L. Bergstrom and J. Edsjo, Phys. Rev. Lett. **99** (2007) 041301 [arXiv:astro-ph/0703512].
- [16] P. Agrawal, E. M. Dolle and C. A. Krenke, Phys. Rev. D **79** (2009) 015015 [arXiv:0811.1798 [hep-ph]]. S. Andreas, M. H. G. Tytgat and Q. Swillens, JCAP **0904** (2009) 004 [arXiv:0901.1750 [hep-ph]]. E. Nezri, M. H. G. Tytgat and G. Vertongen, JCAP **0904** (2009) 014 [arXiv:0901.2556 [hep-ph]].
- [17] E. Lundstrom, M. Gustafsson and J. Edsjo, Phys. Rev. D **79** (2009) 035013 [arXiv:0810.3924 [hep-ph]].
- [18] Q. H. Cao, E. Ma and G. Rajasekaran, Phys. Rev. D **76**, 095011 (2007) [arXiv:0708.2939 [hep-ph]]. T. Hambye, F. S. Ling, L. Lopez Honorez and J. Rocher, JHEP **0907**, 090 (2009) [arXiv:0903.4010 [hep-ph]]. C. Arina, F. S. Ling and M. H. G. Tytgat, JCAP **0910** (2009) 018 [arXiv:0907.0430 [hep-ph]]. E. Dolle, X. Miao, S. Su and B. Thomas, arXiv:0909.3094 [hep-ph].
- [19] C. E. Yaguna, Phys. Rev. D **81** (2010) 075024 [arXiv:1003.2730 [hep-ph]].
- [20] L. L. Honorez and C. E. Yaguna, JHEP **1009**, 046 (2010) [arXiv:1003.3125 [hep-ph]].
- [21] A. Pierce and J. Thaler, JHEP **0708**, 026 (2007) [arXiv:hep-ph/0703056].
- [22] M. E. Peskin and T. Takeuchi, Phys. Rev. D **46** (1992) 381.
- [23] http://lepewwg.web.cern.ch/LEPEWVG/plots/summer2005/s05_stu_contours.eps
- [24] G. Belanger, F. Boudjema, A. Pukhov and A. Semenov, Comput. Phys. Commun. **176** (2007) 367 [arXiv:hep-ph/0607059]. G. Belanger, F. Boudjema, A. Pukhov and A. Semenov, arXiv:0803.2360 [hep-ph]. G. Belanger, F. Boudjema, A. Pukhov and A. Semenov, Comput. Phys. Commun. **174** (2006) 577 [arXiv:hep-ph/0405253]. G. Belanger, F. Boudjema, A. Pukhov and A. Semenov, Comput. Phys. Commun. **149** (2002) 103 [arXiv:hep-ph/0112278].
- [25] M. Cirelli, N. Fornengo and A. Strumia, Nucl. Phys. B **753**, 178 (2006) [arXiv:hep-ph/0512090].
- [26] T. Hambye and M. H. G. Tytgat, Phys. Lett. B **659**, 651 (2008) [arXiv:0707.0633 [hep-ph]].
- [27] S. Andreas, T. Hambye and M. H. G. Tytgat, JCAP **0810**, 034 (2008) [arXiv:0808.0255 [hep-ph]].
- [28] S. Andreas, M. H. G. Tytgat and Q. Swillens, JCAP **0904**, 004 (2009) [arXiv:0901.1750 [hep-ph]].

- [29] C. Arina, F. S. Ling and M. H. G. Tytgat, JCAP **0910**, 018 (2009) [arXiv:0907.0430 [hep-ph]].
- [30] E. Nezri, M. H. G. Tytgat and G. Vertongen, JCAP **0904**, 014 (2009) [arXiv:0901.2556 [hep-ph]].
- [31] R. Bernabei *et al.* [DAMA Collaboration], Eur. Phys. J. C **56**, 333 (2008) [arXiv:0804.2741 [astro-ph]].
- [32] C. E. Aalseth *et al.* [CoGeNT collaboration], arXiv:1002.4703 [astro-ph.CO].
- [33] T. Hambye, F. S. Ling, L. Lopez Honorez and J. Rocher, JHEP **0907**, 090 (2009) [Erratum-ibid. **1005**, 066 (2010)] [JHEP **1005**, 066 (2010)] [arXiv:0903.4010 [hep-ph]].
- [34] Q. H. Cao, E. Ma and G. Rajasekaran, Phys. Rev. D **76**, 095011 (2007) [arXiv:0708.2939 [hep-ph]].
- [35] E. Dolle, X. Miao, S. Su and B. Thomas, Phys. Rev. D **81**, 035003 (2010) [arXiv:0909.3094 [hep-ph]].
- [36] X. Miao, S. Su and B. Thomas, Phys. Rev. D **82**, 035009 (2010) [arXiv:1005.0090 [hep-ph]].
- [37] Z. Ahmed *et al.* [The CDMS-II Collaboration], Science **327** (2010) 1619 [arXiv:0912.3592 [astro-ph.CO]].
- [38] E. A. Baltz and P. Gondolo, JHEP **0410** (2004) 052 [arXiv:hep-ph/0407039].
- [39] R. R. de Austri, R. Trotta and L. Roszkowski, JHEP **0605** (2006) 002 [arXiv:hep-ph/0602028].
- [40] J. R. Ellis and K. A. Olive, Phys. Lett. B **514** (2001) 114 [arXiv:hep-ph/0105004].
- [41] H. Baer and A. D. Box, Eur. Phys. J. C **68** (2010) 523 [arXiv:0910.0333 [hep-ph]].
- [42] [CDF and D0 Collaboration], arXiv:1007.4587 [hep-ex].
- [43] C. Amsler *et al.* [Particle Data Group], Phys. Lett. B **667** (2008) 1.
- [44] R. Catena and P. Ullio, JCAP **1008**, 004 (2010) [arXiv:0907.0018 [astro-ph.CO]].
- [45] J. F. Navarro, C. S. Frenk and S. D. M. White, Astrophys. J. **462**, 563 (1996) [arXiv:astro-ph/9508025].
- [46] A. A. Abdo *et al.* [The Fermi-LAT collaboration], Phys. Rev. Lett. **104**, 101101 (2010) [arXiv:1002.3603 [astro-ph.HE]]. A. A. Abdo *et al.* [Fermi LAT Collaboration], Phys. Rev. Lett. **103** (2009) 251101 [arXiv:0912.0973 [astro-ph.HE]].
- [47] M. Cirelli, P. Panci and P. D. Serpico, Nucl. Phys. B **840** (2010) 284 [arXiv:0912.0663 [astro-ph.CO]]. A. A. Abdo *et al.* [Fermi-LAT Collaboration], JCAP **1004** (2010) 014 [arXiv:1002.4415 [astro-ph.CO]]. G. Hutsi, A. Hektor and M. Raidal, JCAP **1007** (2010) 008 [arXiv:1004.2036 [astro-ph.HE]].
- [48] E. Aprile [Xenon Collaboration], J. Phys. Conf. Ser. **203** (2010) 012005.